Shell effect driven fission modes in fragment mass and total kinetic energy distribution of ^{192}Hg*

Rishabh Kumar,[1] Moumita Maiti,[1,*] A. Pal,[2,3] Satyaranjan Santra,[2,3] Pavneet Kaur,[1] Malvika Sagwal,[1] Ankur Singh,[1] Prakash Chandra Rout,[2,3] Abhijit Baishya,[2] Ramandeep Gandhi,[2,3] and Telagasetti Santhosh[2]

[1]*Department of Physics, Indian Institute of Technology Roorkee, Roorkee 247667, Uttarakhand, India*

[2]*Nuclear Physics Division, Bhabha Atomic Research Centre, Mumbai 400085, India*

[3]*Homi Bhabha National Institute, Anushaktinagar, Mumbai 400094, India*

(Received 8 December 2022; accepted 10 March 2023; published 24 March 2023)

Background: Asymmetric fission in sublead nuclei, especially mercury and platinum isotopes, has generated keen interest in studying fission in $A < 200$ mass region. The role of proton and neutron shells on asymmetric fission in these nuclei is still under test and requires more investigation.

Purpose: This paper presents measurements aimed at studying the fission modes of ^{192}Hg formed in the reaction ^{32}S + ^{160}Gd in the excitation energy range 54–74 MeV.

Method: Mass distributions have been determined from the fission fragments' (FF) time of flight (TOF). Two multiwire proportional chambers were placed symmetrically on opposite sides of the beam to cover the folding angle for symmetric fission. The measured TOF of the fission fragments was used to obtain their velocities, and after clean separation of compound nuclear fission events, the velocities were further used to obtain the fission fragment mass and total kinetic energy (TKE) distribution.

Results: The fission fragment mass distributions at all beam energies were found to be characteristically flat topped, which deviates significantly from a single Gaussian behavior. The distinctive features of mass and energy distributions happen to be explained by the presence of a symmetric fission mode and three asymmetric fission modes, manifested by different total kinetic energies in varying mass regions. These asymmetric fission modes are a consequence of the stabilization role of proton shells at $Z \approx 36$, $Z \approx 46$, and $Z = 28/50$. The most probable mass of light and heavy fragments are found to be around 86 and 106 u, respectively. The symmetric yield is found to increase with the excitation energy.

Conclusions: The present study indicates a mixture of symmetric and asymmetric modes in the fission of ^{192}Hg nuclei and points out the relevance of deformed proton shells at $Z \approx 36$ and 46.

DOI: 10.1103/PhysRevC.107.034614

I. INTRODUCTION

The fission of preactinides has recently witnessed considerable development both experimentally and theoretically [1]. In a decade since the discovery of asymmetric split in β-delayed fission of ^{180}Tl [2] and complementary follow-up heavy-ion experiments on fission of neutron-deficient mercury isotopes [3,4], a qualitative understanding of the complex fission process in sublead nuclei has been achieved. However, an extensive understanding of the role of shell effects on the fission process in preactinides and its connection with shell effects in actinides is a vital question in nuclear fission studies today. Such efforts are also demanded since fission plays a vital role in the astrophysical *r* process [5], the creation of heavy and medium nuclei far from stability [6,7], power production, and the synthesis of application-based radio isotopes.

In the early fission studies of preactinides ($Z < 89$), the split was primarily thought of as symmetric due to weak shell corrections to the macroscopic potential for these nuclei [8]. However, later investigations showed mass distributions deviating significantly from a single Gaussian, indicating the presence of asymmetric fission in preactinides [9,10], which was not expected from the viewpoint of the liquid drop model (LDM). Although the transition-state method with empirical shell corrections to the mass-symmetric fission valley was used to describe the mass distributions, the nature of shell corrections and their dependence on the proton and neutron numbers remained unanswered. The asymmetric fission in ^{180}Hg has renewed the experimental [3,4,11–20] and theoretical interest [21–27] in the fission of sublead nuclei since the concept of shell effects demanded splitting of ^{180}Hg into a symmetric channel (semimagic ^{90}Zr, $Z = 40$ and $N = 50$). An empirical investigation of the experimental data has provided evidence of the dominant proton shell effect for $Z \approx$ 34–38 in the light fragment and $Z \approx 44$–46 in the heavy fragment driving the asymmetric fission in $A \leqslant 200$ nuclei [28]. Thus, it has been recently put forth that similar to the actinides, asymmetric fission in preactinides is also driven by proton shells [27]. However, the proton and neutron shells driving different fission mode has not been unambiguously identified for the lighter preactinides.

The transition of a compound nucleus (CN) from the ground state over the fission barrier to the scission point, leading to its splitting into two fragments, is due to a subtle interplay of collective (macroscopic) and single-particle

*Corresponding author: moumita.maiti@ph.iitr.ac.in

TABLE I. Some of the relevant quantities for the fission reaction $^{32}S + ^{160}Gd$ populating $^{192}Hg^*$ CN, such as the beam energy in laboratory frame (E_{lab}); the ratio of beam energy in center-of-mass frame to the Bass barrier [32] ($E_{c.m.}/V_B$); the initial excitation energy of the compound nucleus (E^*_{CN}); the mean angular momentum ($\langle\ell\rangle$); the angular momentum dependent fission barrier [33] [$B_f(\langle\ell\rangle)$]; the energy loss due to prescission neutron emission (E_{pre}); the rotational energy (E_{rot}) and excitation energy at the saddle point(E^*_{SP}); the standard deviation of mass distribution (σ_M^{LDM}), estimated via systematics based on the LDM [34]; and the total kinetic energy for the symmetric mass split estimated using the Viola systematics [35] (TKE_{VIOLA}) are listed.

E_{lab} (MeV)	$E_{c.m.}/V_B$	E^*_{CN} (MeV)	$\langle\ell\rangle$ ($\hbar$)	$B_f(\langle\ell\rangle)$ (MeV)	E_{pre} (MeV)	E_{rot} (MeV)	E^*_{SP} (MeV)	σ_M^{LDM} (u)	TKE_{VIOLA} (MeV)
139.7	0.97	54.2	24	11.46	15.24	3.08	24.5	12.0	139.2
151.9	1.06	64.6	31	10.37	21.82	5.11	27.3	12.3	
163.3	1.14	74.3	38	8.95	27.92	7.63	29.7	12.8	

(microscopic) effects. This leads to a fission that is strongly influenced by the shell effects residing in the fissioning nucleus and the nascent fragments. Actinides are known to be dominated by $Z \approx 52$–56 deformed proton shells leading to a constant heavy fragment mass of around 142–144. Recently, it has been argued that octupole (pear-shaped) stabilized deformed shell gaps are relevant in predicting the fission properties of actinides [29]. This has been surprisingly found to prevail in the nuclei lighter than lead too, where octupole correlations induced by deformed shell gaps at $N = 52$–56 neutrons and those associated with large quadrupole deformations at 34 and 42–46 proton numbers drive the asymmetric fission [27].

Asymmetric fission in mercury (Hg) isotopes has been of particular interest, and the fission study of neutron-deficient mercury isotopic chain has revealed some intriguing features. It has been shown that asymmetric fission in $^{180,182,183,190}Hg$ is persistent to exist even at high excitation energies ($E^*_{CN} > 50$ MeV) [3,19] which is quite in contrast to what is known for actinide nuclei. Apart from this, the fission in Hg isotopes becomes more symmetric with increasing neutron number. For example, mass distribution for $^{195,196,198}Hg$ formed in $^{12,13}C + ^{182,184,186}W$ reactions primarily follow a symmetric channel for fission [4,17]. The transition from asymmetric to symmetric distribution in this isotopic chain occurs near $^{190}Hg - ^{194}Hg$, where only one measurement is available. Excited ^{192}Hg CN populated via $^{12}C + ^{180}W$ revealed the mass distribution to be slightly flat topped but more towards a symmetric type (even at low E^*_{CN} of 35.8 MeV). Anew, when populating the same CN via two different entrance channels with differing mass asymmetry, the mass distributions for reactions with more asymmetric reaction partners is broader and possess structures attributed to asymmetric fission [15,30] in comparison to those having more symmetric reaction partners. Furthermore, these observations were connected to fission fragments from a noncompound process called quasifission. Strong signatures of quasifission were recently reported for ^{180}Hg formed in the $^{68}Zn + ^{112}Sn$ reaction, and it was concluded that the threshold value of $Z_P Z_T = 1450 \pm 100$ for quasifission appearance in $Z_{CN} = 80$ region holds true [31].

Hence, with so many intricate processes affecting the fission in sublead nuclei, a clear understanding of the complex fission process is still not at our doorstep. The present study tries to decipher different fission modes in ^{192}Hg ($N/Z = 1.4$) formed via the $^{32}S + ^{160}Gd$ reaction at energies mentioned in Table I. The experimental details are provided in Sec. II, results are discussed in Sec. III, and Sec. IV concludes the report.

II. EXPERIMENTAL DETAILS

Fission fragments for the $^{32}S + ^{160}Gd$ reaction were measured using pulsed ^{32}S beam with energy ranging from 139.7 to 163.3 MeV at the 14-UD BARC-TIFR Pelletron-Linac facility, Mumbai, India. The time interval between the bunches was 106.7 ns. The time structure of the bunch was monitored continuously by detecting γ rays in a BaF_2 detector placed at the beam dump. The typical width (full width at half maximum) of the bunch was ≈1.0 ns. An enriched ^{160}Gd (enrichment: 98.2%) target with thickness ≈50 μg/cm^2 was employed, supported by a layer of ^{12}C with thickness ≈ 20 μg/cm^2. To detect the fission fragments in coincidence, two position-sensitive multiwire proportional chambers (MWPCs), each with an active area of 12.5 cm × 7.5 cm, were stationed at folding angles, at 27.5 and 28 cm from the target center [36]. The detectors were placed symmetrically around the beam direction to cover the folding angle for symmetric fission of $\theta = 134^\circ$, with each detector having an angular acceptance of ≈ ±12°; a schematic diagram of the experimental setup is displayed in Fig. 1. The time of flight (TOF) was recorded with respect to the arrival of the beam pulse. The

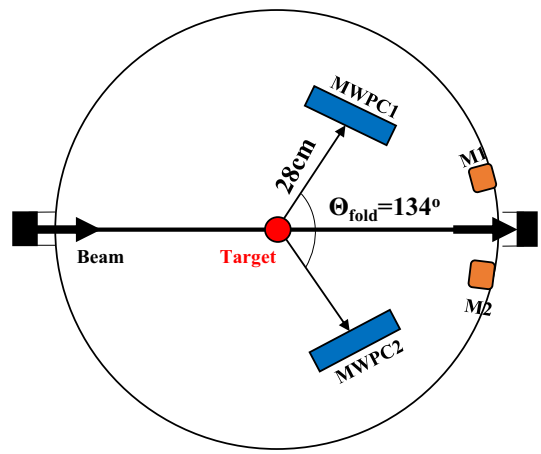

FIG. 1. A schematic diagram of the experimental setup used to measure fission fragment mass distribution of $^{32}S + ^{160}Gd$ system.

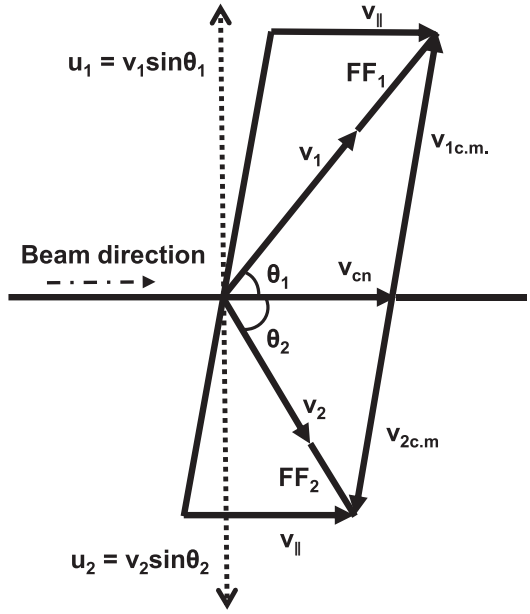

FIG. 2. Kinematics of symmetric binary fission from the compound nucleus.

radio-frequency signal from the beam buncher filtered by the OR of the MWPC cathode signals was used as the arrival time of the beam pulse. The timing correlation spectrum of the two particles detected in coincidence allows for a clear distinction of the fission fragments from other elastic or quasielastic events, as shown in Fig. 3(a). The scattering angle θ and azimuthal angle ϕ of the fission fragments were determined on an event-by-event basis after the position spectra were calibrated using the data with masks of known dimensions kept in front of the detectors. A precision time calibrator was utilized to perform timing calibration; this device creates two signals, one of which is used as a START signal and the other as a STOP signal after an appropriate known delay. Use of a time calibrator gave us the slope of a linear relationship between the channel number and time. However, the time offset t_0 and the electronic delay (δt_0) between the two detectors were obtained, as discussed below.

According to Refs. [37,38], the t_0 and δt_0 can be obtained by meeting the following requirements: (i) the velocity of the fissioning system in the beam direction ($v_\parallel$) should equal the recoiling velocity of the compound nucleus or $v_\parallel - v_{cn} = 0$ and (ii) mass distribution, which is obtained by taking the ratio of FF velocities ($v_{1c.m.}$, $v_{2c.m.}$) in the center-of-mass (c.m.) frame, should be reflection symmetric around $A_{CN}/2$. Here $v_{1c.m.}$ and $v_{2c.m.}$ are the fission fragment center-of-mass velocities corresponding to masses m_1 and m_2, respectively. The expressions for $v_\parallel$, $v_\perp$ (the velocity component of fissioning nucleus perpendicular to the reaction plane), $v_{1c.m.}$, and $v_{2c.m.}$ are given by [39]

$$v_\parallel = \frac{u_1 w_2 + u_2 w_1}{u_1 + u_2}, \tag{1}$$

$$v_\perp = \frac{u_1 u_2 \sin\phi_{12}}{\sqrt{u_1^2 + u_2^2 - 2u_1 u_2 \cos\phi_{12}}}, \tag{2}$$

$$v_{1c.m.} = \sqrt{v_1^2 + v_{cn}^2 - 2v_1 v_{cn}\cos\theta_1}, \tag{3}$$

$$v_{2c.m.} = \sqrt{v_2^2 + v_{cn}^2 - 2v_2 v_{cn}\cos\theta_2}, \tag{4}$$

where w_1, w_2 and u_1, u_2 are the measured velocity vectors decomposed into orthogonal components parallel and perpendicular to the beam axis, respectively ($w_1 = v_1\cos\theta_1$, $w_2 = v_2\cos\theta_2$, $u_1 = v_1\sin\theta_1$, $u_2 = v_2\sin\theta_1$, where v_1, v_2 and θ_1, θ_2 are the velocities and scattering angles measured with respect to the beam direction, see Fig. 2). ϕ_{12} is the azimuthal folding angle. Energy loss in the target and backing medium has been computed using the Stopping and Range of Ions in

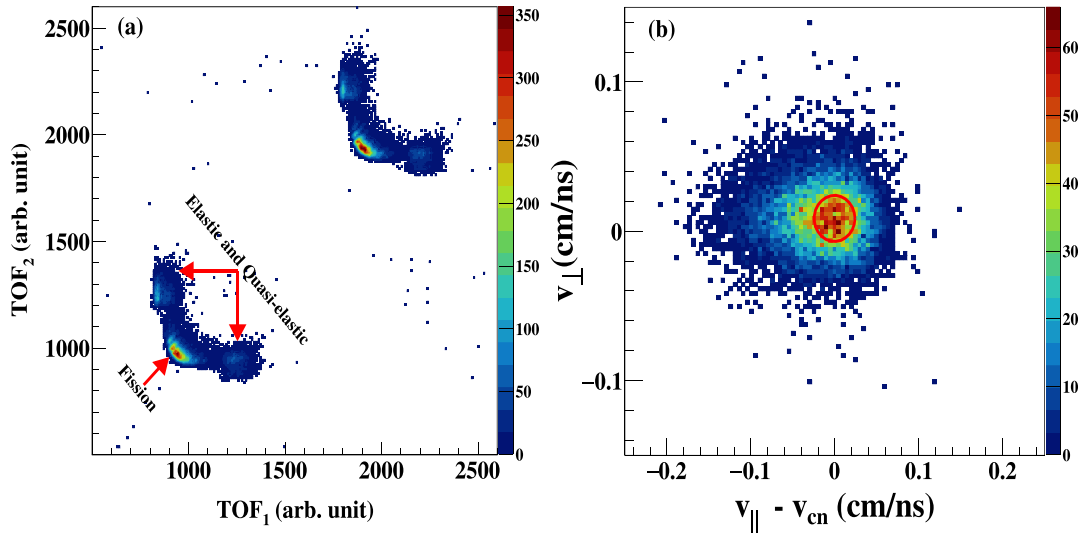

FIG. 3. Typical plots of (a) correlation of time of flights (TOF_1 vs TOF_2) of both fission fragments, cleanly identifying for both the beam pulses and (b) $v_\parallel - v_{cn}$ versus $v_\perp$, obtained for $^{32}S + ^{160}Gd$ reaction at $E_{beam} = 151.9$ MeV. The area inside the red circle corresponds to the binary events following the complete fusion process.

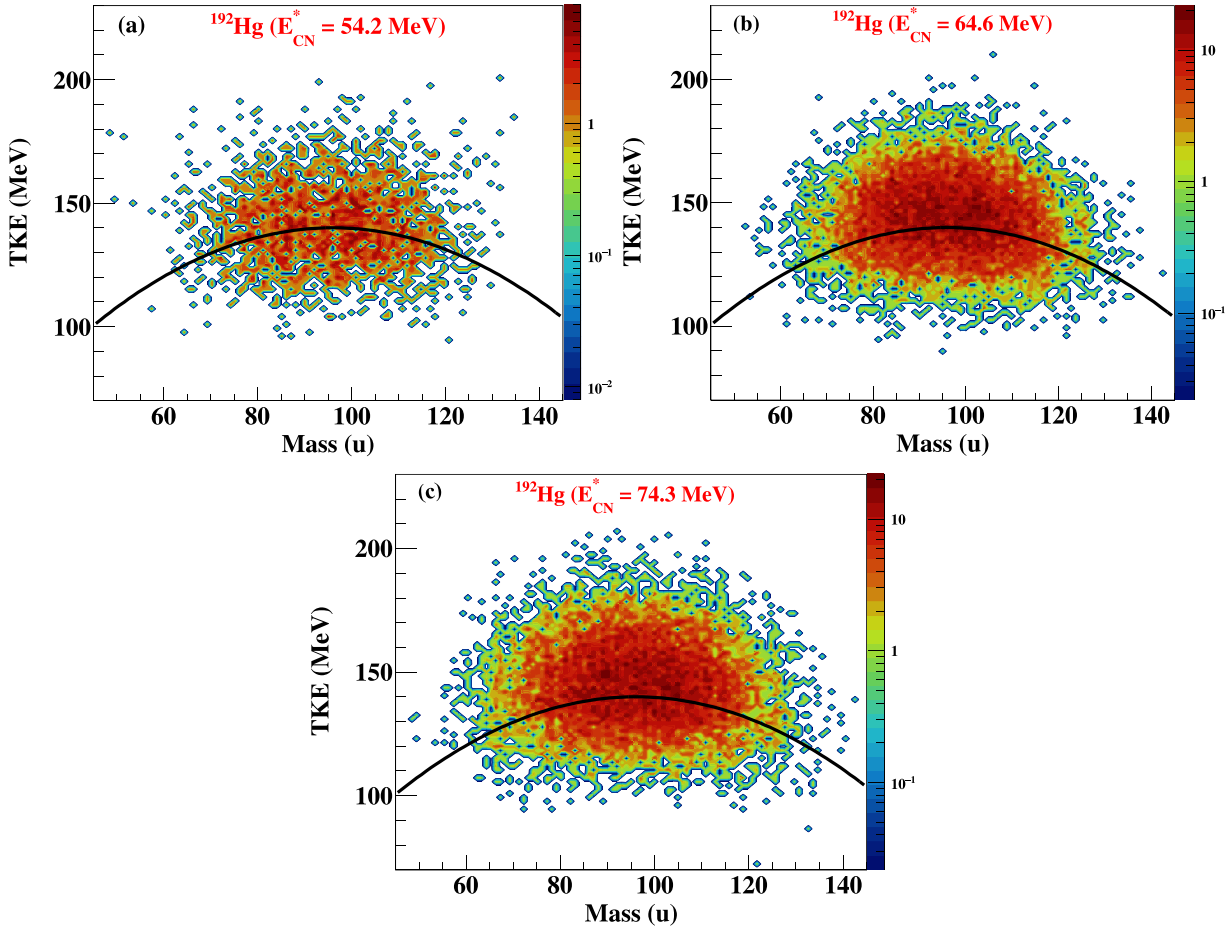

FIG. 4. Mass-TKE correlation obtained for the fissioning nucleus ^{192}Hg populated using $^{32}S + ^{160}Gd$ reaction at E_{beam} = (a) 139.7 MeV, (b) 151.9 MeV, and (c) 163.3 MeV. The black curve represents the parabolic dependence shown in Eq. (9).

Matter code [40] and has been included in the above analysis iteratively. The small target thickness (≈50 μg/cm^2) has a negligible effect on the derived mass and total kinetic energy (TKE) distributions.

Heavy-ion-induced fusion-fission reactions always carry a possibility of transfer-induced fission interfering with the complete fusion-fission for beam energies close to or below the Coulomb barrier. A correlation plot of parallel ($v_\parallel$) versus perpendicular ($v_\perp$) components of velocity vectors of the fissioning nucleus is very useful [41,42] to reject the contribution of transfer fission. A typical two-dimensional plot for $v_\parallel - v_{cn}$ versus $v_\perp$ is shown in Fig. 3(b) for 151.9 MeV beam energy, where both $v_\perp$ and $v_\parallel - v_{cn}$ for the majority of the events were observed around 0.0, which corresponds to a full momentum transfer (FMT). The events within the red circle (of radius ≈ 0.02 cm/ns) in Fig. 3(b) should correspond to the binary events followed by FMT, and only these events have been analyzed to derive the mass and TKE distributions. The scattered events outside the gate have contributions from transfer-induced fission or partial momentum transfer events.

The masses and total kinetic energy of the fragments have been determined event by event using the measured velocities of the fission fragments and employing simple two-body kinematics for binary fission [39,43] given by

$$M_1 = \frac{v_{2c.m.} M_{CN}}{v_{1c.m.} + v_{2c.m.}}, \tag{5}$$

$$M_2 = \frac{v_{1c.m.} M_{CN}}{v_{1c.m.} + v_{2c.m.}}, \tag{6}$$

$$\text{TKE} = \frac{1}{2} M_1 v^2_{1c.m.} + \frac{1}{2} M_2 v^2_{2c.m.}, \tag{7}$$

where compound nucleus mass is the sum of the projectile and target masses ($M_{CN} = A_P + A_T$). The fission events of both lobes in the TOF-TOF spectrum [in Fig. 3(a)] have been used to deduce the mass-energy distributions. The mass resolution or σ (standard deviation) of the experimental setup was estimated to be ≈4 u by using the kinematical method proposed by Biswas *et al.* [43].

III. RESULTS AND DISCUSSION

A. Mass and energy distributions of fission fragments

Mass-total kinetic energy (M-TKE) distributions of the primary binary fragments obtained in the $^{32}S + ^{160}Gd$ reaction leading to the formation of $^{192}Hg^*$ CN at lab energies 139.7, 151.9, and 163.3 MeV are shown in Fig. 4. The pure

fissionlike products obtained and shown in the M-TKE plots are characterized by large mass transfer and energy dissipation and originate from the CN fission or quasifission process. One can assess QF probability based on mean fissility parameter χ_m, expressed as $\chi_m = 0.25\chi_{\rm CN} + 0.75\chi_{\rm eff}$, where $\chi_{\rm CN}$ is the fissility of compound nucleus and $\chi_{\rm eff}$ is the effective fissility parameter reflecting the entrance channel mass and charge asymmetry [44]. From a systematic analysis of mass-angle distributions for numerous reactions, it is known that QF appears for reactions with $\chi_m > 0.68$, resulting in the widening of mass distributions and forward-backward asymmetry in angular distributions. A value of 0.6 for χ_m has been obtained for the present reaction studied. This value turns out to be less than the threshold value for QF appearance. It means that the studied reaction is more favorable for compound nuclear fission. Quasifission was not observed for reactions with similar χ_m values in some previous studies [3,18].

It can be noted from Table I that the reaction was studied at energies 14% above the Coulomb barrier to 3% below the barrier, and thus the fission process in ^{192}Hg could be investigated in the 54 to 74 MeV excitation energy range. The prescission neutron and proton emission takes away some part of the initial $E^*_{\rm CN}$ at such high excitation energies. Thus, the actual fissioning isotope and its excitation energy may differ from the initial compound nucleus, especially at such high excitation energies where the influence of prescission emission is the strongest. The prescission proton multiplicities calculated with NRV code [45] were found to be at least three times less than the neutron multiplicities, which were estimated using the systematics [34,46]. Hence, the proton emission before scission may be neglected in our case. Since preactinides have substantial deformations in the transition states (saddle point), a dumbbell-like shape with a thin neck close to the scission point is proper to these large deformations, and the influence of dynamic effects on the descent from the saddle to the scission point is thought to be comparatively smaller than the actinides [27]. The fission properties of these nuclei are mainly determined at the saddle point and depend on their excitation energy, which is defined as a simple approximation as follows:

$$E^*_{\rm SP} = E^*_{\rm CN} - B_f(\langle\ell\rangle) - E_{\rm pre} - E_{\rm rot}, \tag{8}$$

where $B_f(\langle\ell\rangle)$ is the angular momentum–dependent fission barrier (since the mean angular momentum induced by the ^{32}S projectile is relatively large (see Table I), a rotating liquid drop fission barrier is used [33]), $E_{\rm pre}$ is the energy carried away by the prescission neutrons, and $E_{\rm rot}$ is the rotational energy of the fissioning nucleus at the saddle point. The values of beam energy, corresponding excitation energies of the CN, mean angular momentum of CN obtained from CCFULL [47], fission barrier at these $\langle\ell\rangle$s, and excitation energies at the saddle point for the studied reaction are listed in Table I.

It can be noted from Fig. 4 that the mass-energy distributions are typical of LDM behavior owing to the high excitation energies obtained in the ^{32}S + ^{160}Gd reaction. However, one can see some peculiar structures in the M-TKE at the lowest excitation energy (54.2 MeV) that are less pronounced compared to the observations in ^{180,182,183}Hg [19] at the lowest studied excitation energy; this could be due to the lower $E^*_{\rm CN}$ achieved in the latter nuclei via heavy-ion-induced reactions compared to our case. However, the M-TKE of ^{192}Hg at $E^*_{\rm CN} = 54.2$ MeV resembles the one for ^{190}Hg nuclei studied at $E^*_{\rm CN} = 56.7$ MeV via the ^{36}Ar + ^{154}Sm reaction [18]. Note that the M-TKE has a parabolic relationship, as shown in the M-TKE plots (see Fig. 4).

The fission fragment mass distributions (FFMD) of excited ^{192}Hg at three excitation energies normalized to 200% are presented in the left panels of Fig. 5. The mass distributions are flat topped in the symmetric mass region (a known characteristic now in the fission of nuclei in the neutron-deficient lead island) at the two lower beam energies and almost single peaked at the highest one. However, we can see an apparent dip in the mass distribution around the mass symmetry at the lowest excitation energy. The mass distributions move toward a more symmetric one as we increase the excitation energy. Based on the small kinks found at mass 86 and 106 u in the FFMD at $E^*_{\rm CN} = 54.2$ MeV ($E^*_{\rm SP} = 24.5$ MeV), these masses can be regarded as the most probable mass of the light and heavy fragments, respectively. Furthermore, the mass distribution is found to be broader than the one obtained for ^{192}Hg-excited CN formed in the ^{12}C + ^{180}W reaction [17]. Interestingly, the flat-top behavior exists at high excitation energies ($E^*_{\rm CN} \approx$ 65 MeV) also, indicating the persistence of asymmetric channel even at high excitation energy, a behavior observed by Nishio *et al.* in the fission of ^{180,190}Hg [3].

A quick look at the mass distributions (see left panels of Fig. 5) at the three energies show that they can be deconvoluted into one symmetric and one or more asymmetric modes. The TKE distributions of fission fragments for different mass ranges (symmetric mass division $A_{\rm CN}/2 \pm 5$ u, the mass range where the maximal yield of asymmetric modes is found, i.e., 76–91 u, and very asymmetric fragments with masses 56–76 u) are shown in the right panels of Fig. 5. However, the TKE distributions possess a complex structure and change significantly with fragment mass. Recently, Bogachev *et al.* [18] and Kozulin *et al.* [19], proposed the method of decomposing mass distribution with different asymmetric fission modes and symmetric mode based on the presence of several components with vastly different mean energies in the TKE distribution of Hg, Pt, and Pb isotopes. Also, it has been recently put forth that multiple deformed neutron and proton shells can drive asymmetric fission in preactinides, especially in $A \leqslant 200$ nuclei [27,28]. Thus, the obtained mass and TKE distributions in the present study can also be analyzed similarly to those proposed in Refs. [18,19] depending on the structure of TKE distribution observed for different mass ranges. The mass distributions will be discussed right after the TKE distribution to get the relevant details of the fission modes.

The TKE distributions of ^{192}Hg* fissioning nucleus at excitations $E^*_{\rm SP} = 29.7$, 27.3, and 24.5 MeV for 91–101 u, 76–91 u, and 56–76 u are presented in Figs. 5(d)–5(l). Notably, the TKE distributions are not single Gaussian but have peculiar structures. Now, according to the LDM, the TKE of fission fragments is independent of CN excitation energy but has a parabolic dependence on the fragment mass,

$$\mathrm{TKE}(M) = 4 \times \mathrm{TKE}_{\rm Viola} \times \frac{M(M_{\rm CN} - M)}{M^2_{\rm CN}}, \tag{9}$$

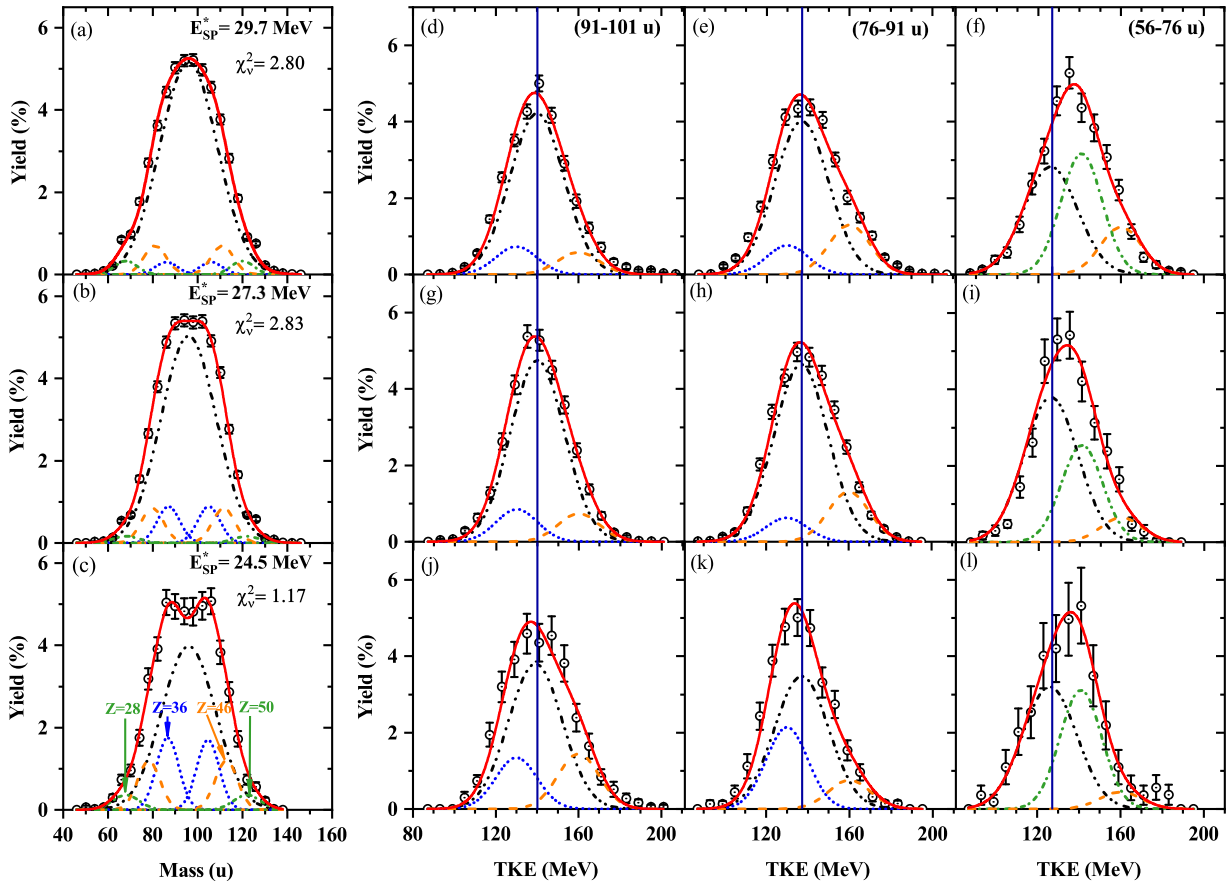

FIG. 5. Left: Fission fragment mass distributions for ^{192}Hg formed in the ^{32}S + ^{160}Gd reaction at $E_{\rm beam}$ = (a) 163.3 MeV, (b) 151.9 MeV, and (c) 139.7 MeV. The χ^2 per degree of freedom, i.e., χ^2_ν (reduced chi-square), is presented for each fit. Right: The TKE distribution of fission fragments for different mass regions [(d)–(l)] corresponds to each mass distribution shown in the left panel. The lines correspond to the decomposition of TKE and mass distributions into the symmetric (black dashed-dot-dotted line), asymmetric A1 (blue dotted line), asymmetric A2 (orange dashed line), and asymmetric A3 (green dashed-dotted line) fission modes. The red line represents the superposition of all the modes, and vertical lines in each TKE panel indicate the mean TKE value estimated using Viola systematics [35].

where M is fragment mass and $\rm TKE_{Viola}$ is the most probable TKE estimated using the Viola systematics [35]. The vertical blue lines in the TKE panels of Fig. 5 indicate the expected TKE values for symmetric mode in a given fragment mass range. It has been brought out by the systematic study of fission fragment mass and energy distributions of excited nuclei [34] that for nuclei with $Z^2/A^{1/3} \approx 1100$, the standard deviation of TKE distribution is about 9.5–10 MeV. Now, keeping in mind the energy resolution of the present measurements, we can expect the standard deviation of the TKE distribution for the symmetric mode to be about 11 MeV. An additional reason to use a σ value of TKE for the symmetric mode from systematics is the inability to explicitly measure this value from present measurement since multiple fission modes are supposed to exist in ^{192}Hg* fission.

If we shed our focus on the TKE panels for the symmetric mass range 91–101 u at all three excitation energies, then one can observe a slight deviation of TKE distribution from a single Gaussian shape as expected from the LDM. This deviation is most markedly seen at the lowest excitation energy ($E^*_{\rm SP}$ = 24.5 MeV). Let us see these peculiarities by taking TKE distributions at the lowest excitation energy as an example. For the symmetric mass split [see Fig. 5(j)], we observe that a single Gaussian with a large standard deviation would approximately fit the data. However, if we consider that for symmetric mode we need a σ around 11 MeV, then multiple Gaussians are required to fit the data correctly. Hence, we need a narrow component with a mean energy of about 130 MeV, which is lower than the expected TKE of about 140 MeV for symmetric mode (blue vertical line) according to LDM to fit the lower TKE side. The fitting procedure shows that the standard deviation of the lower TKE component (blue dotted curve) is $\approx$9 MeV, whereas the broader component (black dashed-dot-dotted curve) with $\sigma \approx 11$ MeV is centered at an energy of 140 MeV which is close to the one estimated by Viola systematics (139.2 MeV). Similar properties of TKE distributions were recently observed in Refs. [18,19]. It has been shown from the study of multimodal fission in actinides [48] that the variance of TKE distributions for the asymmetric modes arising as a consequence of the shell effects is smaller than that for symmetric mode based on LDM. This paves the way for the inclusion of A1 asymmetric mode (blue dotted line) corresponding to the low TKE component observed and also as suggested by Kozulin *et al.* [19]. Furthermore,

another slightly narrower component ($\sigma \approx 8$ MeV) with a mean TKE around 160 MeV (greater than the Viola estimated TKE) exists. These low and high TKE components are also present, complementing the symmetric component in TKE distribution for more asymmetric fission mass range (76–91 u), see Fig. 5(k). Thus, an asymmetric mode A2 (orange dashed curve) is also required to define the fission configuration.

Interestingly, from Fig. 5(l), it can be noted that for the case of very asymmetric fission mass range (56–76 u), the maximum of TKE distribution lies about 14 MeV higher than the TKE for symmetric LDM mode. This distribution corresponding to the maximum peak is narrower than that expected from LDM. In this mass range, the number of protons in fission fragments is close to the proton shells at $Z = 28$ and 50. The proton shell at $Z \approx 52$ has been found to drive asymmetry in the fission of actinide nuclei [49]. Since this shell may also affect the fission of preactinides as the complementary light and heavy fragments in the very asymmetric mass region are close to the proton shell at $Z = 28$ and 50, respectively, another asymmetric mode A3 (green dash-dotted curve) corresponding to this shell seems reasonable to incorporate. The analysis of TKE distributions at the other two higher excitation energies is similar to what we have just discussed. However, the component corresponding to the LDM becomes more dominant with increasing excitation energy. Thus, from the trends observed in the TKE distribution and following the method proposed by Bogachev *et al.* [18] and Kozulin *et al.* [19], the fission in Hg (along with other preactinide nuclei) can be assumed consisting of one symmetric (S) and three asymmetric modes (A1, A2, and A3). The A1 mode is associated with nearly symmetric low-energy fragments, the A2 mode is with high-energy fragments in the 76–91 u mass range, and the A3 mode arises for very light asymmetric fragments (56–76 u).

Since preactinides are known to fission mainly via the symmetric mode as has been evident from many studies [16,19,30,34,48], it is advisable to fix the variance of symmetric mode based on LDM in the fitting procedure of the mass distributions. We have used the empirical systematics based on the LDM [34] to obtain the variance of the S mode for different excitation energy, which is reported in Table I. Depending on the CN excitation energy, the widths of Gaussian associated with different asymmetric modes varied in the range of 4–6 u. The work of Andreyev *et al.* reported mass widths of 4 u for the asymmetric mass distribution of ^{180}Hg from the β-delayed fission of ^{180}Tl [2]. The initial Gaussian parameters for the asymmetric modes were taken to conform with the decomposition of TKE distributions (contributing to each mode in mass distribution close to those in TKE ones). It is worth noting that the fission fragment mass distributions are reasonably well fitted by considering different asymmetric and symmetric modes, as seen in Figs. 5(a)–5(c). The χ^2_ν, i.e., the χ^2 per degree of freedom, are observed to be near $\sim$1, which depicts the good fitting of the mass distribution with the constraints used above. Further, it can also be observed that the contribution of symmetric S mode increases with the excitation energy as expected. The most probable masses and TKEs for each mode are presented in Table II. The neutron and proton numbers were estimated based on the unchanged charge distribution (UCD) assumption, which states that the charge ratio (Z/A) of the fissioning nucleus is retained in the nascent fragments [50]. The experimental mass resolution and prescission neutron emission may add uncertainties up to ± 2 u in the obtained proton and neutron numbers for the different asymmetric modes. The accuracy of obtained TKE values is about ± 3 MeV, including the statistical and systematic errors of measurements.

TABLE II. The most probable masses ($M_{L,H}$) and deduced proton ($Z_{L,H}$), and neutron ($N_{L,H}$) numbers of light and heavy fragments along with the TKE of symmetric (S) and the asymmetric (A1, A2, and A3) fission modes for the ^{192}Hg CN. UCD has been assumed while calculating proton and neutron numbers.

Mode	M_L (u)	M_H (u)	Z_L	Z_H	N_L	N_H	TKE (MeV)
S	96		40		56		140
A1	86.6	105.4	36.0	44.0	50.6	61.4	130
A2	81.0	111.0	33.8	46.2	47.2	64.8	160
A3	70.4	121.0	29.3	50.4	41.1	100.6	141

The extracted proton and neutron numbers for the light and heavy fragments corresponding to the three asymmetric modes are listed in Table II. It can be noted that for A1 mode, $Z_L \approx 36$ and for A2 mode, $Z_H \approx 46$, which are similar to the ones observed for ^{178}Pt, ^{180,182,183,190}Hg, and ^{184,192}Pb [18,19]. Moreover, for the A3 mode, $Z_L \approx 28$ and $Z_H \approx 50$ are the prevalent shells. Recently, it has been argued that $Z \approx 36$, 38 in the light fragments are due to the deformed shell that stabilizes the asymmetric fission in sublead nuclei [17,28]. Also, based on calculations utilizing the Hartree-Fock method with the BCS approximation, the compact $Z_H \approx 42$–46 fragment configuration has also been shown to contribute to the asymmetric fission in Hg and Pt isotopes [27]. In the fission of light thorium isotopes, the symmetric scission was attributed to a compact configuration wherein the number of protons in the formed fragments was found to be $Z = 45$ [51], which can be associated with A2 fission mode in the present study. Last, the A3 mode used for fragments with $Z = 28$ and $Z = 50$ may be connected to the standard I mode at $Z \approx 52$ known in the fission of actinide nuclei [49,52].

A comparison of FFMDs of nuclei in close vicinity of ^{192}Hg viz. ^{190}Hg [18], ^{192}Hg [17], and ^{191}Au [15] at similar excitation energies is presented in Fig. 6. The mass distribution obtained from GEF code [53] calculations at $E^*_{\rm CN} = 54.2$ MeV is also added for comparison. GEF predicts the mass distribution to be more symmetric when compared to the present work. It can be observed that ^{190}Hg (black open squares), ^{191}Au (red open diamonds), and ^{192}Hg (solid blue circles) of the present work have similar mass distribution features, i.e., flat topped and broad. Also, the present mass distribution of ^{192}Hg shows a smaller asymmetric valley at the center as compared to ^{190}Hg, possibly due to more neutrons in ^{192}Hg. Accessing mass distributions of higher neutron excess isotopes of Hg (preferably by a more symmetric entrance

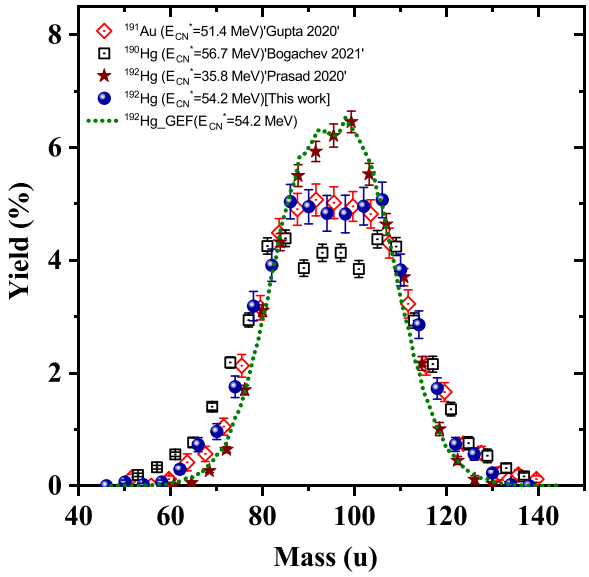

FIG. 6. Comparison of experimental mass distribution of ^{192}Hg (present work) with ^{191}Au (data taken from Gupta *et al.* [15]), ^{190}Hg (data taken from Bogachev *et al.* [18]), and ^{192}Hg (data taken from Prasad *et al.* [17]). GEF predicted mass distribution of ^{192}Hg ($E^*_{\rm CN} = 54.2$ MeV) is also compared with the experimental one. All experimental data are plotted in a bin of 4 amu.

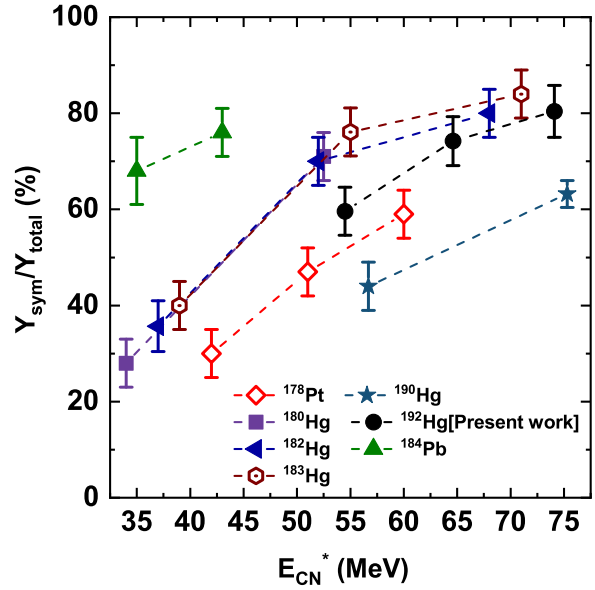

FIG. 7. The contribution of symmetric fission for Pt, Hg, and Pb isotopes in dependence on the initial CN excitation energy. The data for ^{180,182,183}Hg and ^{178}Pt are taken from Ref. [19], and those for ^{190}Hg and ^{184}Pb are taken from Ref. [18].

channel reaction) could possibly confirm this fact and shed more light on the evolution of mass distribution over a wide isotopic chain of Hg. Interestingly, the FFMD of ^{192}Hg formed in ^{12}C + ^{180}W [17] reaction at $E^*_{\rm CN} = 35.8$ MeV is much narrower and single Gaussian type. Investigation into how the ^{192}Hg mass distribution behave at similar or higher excitation energies when populated via two different entrance channel reactions would be interesting.

B. Symmetric mode in the fission of ^{192}Hg and nearby nuclei

The ratio of symmetric yield to the total yield of fission fragments and its dependence on the compound nucleus excitation energy for ^{192}Hg (present work) are compared with ^{180,182,183}Hg [19], ^{178}Pt [19], ^{190}Hg [18], and ^{184}Pb [18] and shown in Fig. 7. Overall, the symmetric mode contribution increases with the excitation energy for all the nuclei. The symmetric yield corresponding to ^{192}Hg is seen to increase linearly in the 60% to 80% range and lies close to the values of ^{182,183}Hg within the error bars. It can also be seen that the slope of increase in the S mode contribution is greater for ^{180,182,183}Hg; as a matter of fact, these are also the nuclei for which one of the lowest excitation energies have been reached. However, for ^{184}Pb, ^{190}Hg, and ^{192}Hg, we observe a rather less rapid increase of symmetric yield with excitation energy. At $E^*_{\rm CN}$ less than 50 MeV, ^{184}Pb is found to have the highest contribution of symmetric mode with 65–75%. It is interesting to note that the two neutron excess isotopes of Hg (^{190,192}Hg) show less symmetric yield as compared to its neutron-deficient isotopes (^{180,182,183}Hg). Moreover, compared to ^{190}Hg, the symmetric yield of ^{192}Hg is significantly higher at similar excitation energies.

IV. CONCLUSION

In the ongoing quest for fission fragment mass and energy distributions of sublead nuclei, the present work provides measurements of fission fragment mass-energy distributions for ^{192}Hg compound nuclei formed in the ^{32}S + ^{160}Gd reaction at $E^*_{\rm SP} = 24.5$, 27.3, and 29.7 MeV. The mass distributions were found to be flat topped in nature, which remained persistent with increasing excitation energy. The distinctive traits in the TKE distributions were interpreted in terms of an admixture of one symmetric LDM component and three asymmetric modes, namely the low-energy component for nearly symmetric fragments, the high-energy one for more asymmetric fragments (76–91 u), and the mid-energy one for very light fragments with masses 56–76 u. These asymmetric modes and the symmetric LDM mode were successfully used to decompose the mass and TKE distributions at all the energies. The analysis of mass and energy distributions to obtain proton and neutron numbers of the most probable light and heavy fragments showed a stabilizing role of proton number $Z \approx 36$ in the light fragment, $Z \approx 46$ in the heavy fragment, and $Z = 28$ and/or 50 in both the light and heavy fragments. Thus, this work suggests the decomposition of mass distribution in $A < 200$ with multiple Gaussians rather than double Gaussian (which discards the presence of an LDM symmetric mode). The experimental mass distributions of ^{192}Hg were found to be similar to those of neighboring nuclei; however, its symmetric yield is higher than that of ^{190}Hg at similar excitation energies, indicating a possible neutron excess effect on the FFMD of Hg isotopes. The excitation energy dependence of the symmetric yield showed an increasing trend for ^{192}Hg as well as other neighboring fissioning nuclei. The degree of increase was found to be different for different nuclei with ^{192,190}Hg showing a slightly weaker dependence of symmetric yield on $E^*_{\rm CN}$, whereas the relatively neutron-deficient Hg

isotopes were found to have a strong dependence. Exploration of asymmetric fission modes in sublead nuclei demands more experimental investigation across a wider span of N/Z ratios to concretely establish the existence of proton-shell-driven fission modes.

ACKNOWLEDGMENTS

The authors thank the BARC-TIFR Pelletron staff for their cooperation and help during the experiment. We also thank the devoted effort of our BARC collaborators and colleagues from the TASISPEC laboratory of IIT Roorkee during the learning period. R.K. acknowledges financial support from the Department of Science and Technology, Ministry of Science and Technology, Government of India, under the INSPIRE fellowship scheme (IF180078). P.K. thanks the UGC, Government of India, for the research fellowship. M.S. and A.S. gratefully acknowledge financial support from MHRD, Government of India. We acknowledge the support of the Department of Atomic Energy, Government of India, under Project Identification No. RTI 4002.

[1] A. N. Andreyev, K. Nishio, and K.-H. Schmidt, Rep. Prog. Phys. **81**, 016301 (2018).
[2] A. N. Andreyev, J. Elseviers, M. Huyse, P. Van Duppen, S. Antalic, A. Barzakh, N. Bree, T. E. Cocolios, V. F. Comas, J. Diriken *et al.*, Phys. Rev. Lett. **105**, 252502 (2010).
[3] K. Nishio, A. N. Andreyev, R. Chapman, X. Derkx, C. E. Düllmann, L. Ghys, F. P. Heßberger, K. Hirose, H. Ikezoe, J. Khuyagbaatar *et al.*, Phys. Lett. B **748**, 89 (2015).
[4] E. Prasad, D. J. Hinde, K. Ramachandran, E. Williams, M. Dasgupta, I. P. Carter, K. J. Cook, D. Y. Jeung, D. H. Luong, S. McNeil *et al.*, Phys. Rev. C **91**, 064605 (2015).
[5] I. Panov, E. Kolbe, B. Pfeiffer, T. Rauscher, K.-L. Kratz, and F.-K. Thielemann, Nucl. Phys. A **747**, 633 (2005).
[6] P. Armbruster, Rep. Prog. Phys. **62**, 465 (1999).
[7] E. Kugler, Hyperfine Interact. **129**, 23 (2000).
[8] F. Plasil, D. S. Burnett, H. C. Britt, and S. G. Thompson, Phys. Rev. **142**, 696 (1966).
[9] M. G. Itkis, N. A. Kondratev, Yu. V. Kotlov, S. I. Mulgin, V. N. Okolovich, A. Y. Rusanov, and G. N. Smirenkin, Sov. J. Nucl. Phys. **47**, 4 (1988).
[10] M. G. Itkis, N. A. Kondratev, S. I. Mulgin, V. N. Okolovich, A. Y. Rusanov, and G. N. Smirenkin, Sov. J. Nucl. Phys. **52**, 601 (1990).
[11] L. Ghys, A. N. Andreyev, M. Huyse, P. Van Duppen, S. Sels, B. Andel, S. Antalic, A. Barzakh, L. Capponi, T. E. Cocolios *et al.*, Phys. Rev. C **90**, 041301(R) (2014).
[12] R. Tripathi, S. Sodaye, K. Sudarshan, B. K. Nayak, A. Jhingan, P. K. Pujari, K. Mahata, S. Santra, A. Saxena, E. T. Mirgule *et al.*, Phys. Rev. C **92**, 024610 (2015).
[13] S. Gupta, C. Schmitt, K. Mahata, A. Shrivastava, P. Sugathan, A. Jhingan, K. S. Golda, N. Saneesh, M. Kumar, G. Kaur *et al.*, Phys. Rev. C **100**, 064608 (2019).
[14] I. Tsekhanovich, A. N. Andreyev, K. Nishio, D. Denis-Petit, K. Hirose, H. Makii, Z. Matheson, K. Morimoto, K. Morita, W. Nazarewicz *et al.*, Phys. Lett. B **790**, 583 (2019).
[15] S. Gupta, K. Mahata, A. Shrivastava, K. Ramachandran, S. K. Pandit, P. C. Rout, V. V. Parkar, R. Tripathi, A. Kumar, B. K. Nayak *et al.*, Phys. Lett. B **803**, 135297 (2020).
[16] B. M. A. Swinton-Bland, M. A. Stoyer, A. C. Berriman, D. J. Hinde, C. Simenel, J. Buete, T. Tanaka, K. Banerjee, L. T. Bezzina, I. P. Carter *et al.*, Phys. Rev. C **102**, 054611 (2020).
[17] E. Prasad, D. J. Hinde, M. Dasgupta, D. Y. Jeung, A. C. Berriman, B. M. A. Swinton-Bland, C. Simenel, E. C. Simpson, R. Bernard, E. Williams *et al.*, Phys. Lett. B **811**, 135941 (2020).
[18] A. A. Bogachev, E. M. Kozulin, G. N. Knyazheva, I. M. Itkis, M. G. Itkis, K. V. Novikov, D. Kumar, T. Banerjee, I. N. Diatlov, M. Cheralu *et al.*, Phys. Rev. C **104**, 024623 (2021).
[19] E. M. Kozulin, G. N. Knyazheva, I. M. Itkis, M. G. Itkis, Y. S. Mukhamejanov, A. A. Bogachev, K. V. Novikov, V. V. Kirakosyan, D. Kumar, T. Banerjee *et al.*, Phys. Rev. C **105**, 014607 (2022).
[20] A. Jhingan, C. Schmitt, A. Lemasson, S. Biswas, Y. H. Kim, D. Ramos, A. N. Andreyev, D. Curien, M. Ciemała, E. Clément, O. Dorvaux *et al.*, Phys. Rev. C **106**, 044607 (2022).
[21] P. Möller, J. Randrup, and A. J. Sierk, Phys. Rev. C **85**, 024306 (2012).
[22] T. Ichikawa, A. Iwamoto, P. Möller, and A. J. Sierk, Phys. Rev. C **86**, 024610 (2012).
[23] A. V. Andreev, G. G. Adamian, and N. V. Antonenko, Phys. Rev. C **86**, 044315 (2012).
[24] M. Warda, A. Staszczak, and W. Nazarewicz, Phys. Rev. C **86**, 024601 (2012).
[25] S. Panebianco, J. L. Sida, H. Goutte, J. F. Lemaître, N. Dubray, and S. Hilaire, Phys. Rev. C **86**, 064601 (2012).
[26] J. D. McDonnell, W. Nazarewicz, J. A. Sheikh, A. Staszczak, and M. Warda, Phys. Rev. C **90**, 021302(R) (2014).
[27] G. Scamps and C. Simenel, Phys. Rev. C **100**, 041602(R) (2019).
[28] K. Mahata, C. Schmitt, S. Gupta, A. Shrivastava, G. Scamps, and K.-H. Schmidt, Phys. Lett. B **825**, 136859 (2022).
[29] G. Scamps and C. Simenel, Nature (London) **564**, 382 (2018).
[30] Kavita, K. S. Golda, T. K. Ghosh, A. Jhingan, P. Sugathan, A. Chatterjee, B. R. Behera, A. Kumar, R. Kumar, N. Saneesh *et al.*, Phys. Rev. C **100**, 024626 (2019).
[31] E. M. Kozulin, E. Vardaci, W. H. Trzaska, A. A. Bogachev, I. M. Itkis, A. V. Karpov, G. N. Knyazheva, and K. V. Novikov, Phys. Lett. B **819**, 136442 (2021).
[32] R. Bass, Nucl. Phys. A **231**, 45 (1974).
[33] A. J. Sierk, Phys. Rev. C **33**, 2039 (1986).
[34] M. G. Itkis and A. Ya. Rusanov, Phys. Part. Nuclei **29**, 160 (1998).
[35] V. E. Viola, K. Kwiatkowski, and M. Walker, Phys. Rev. C **31**, 1550 (1985).
[36] A. Pal, S. Santra, A. Kundu, D. Chattopadhyay, A. Jhingan, B. K. Nayak, and S. Prafulla, J. Instrum. **15**, P02008 (2020).
[37] R. Rafiei, R. G. Thomas, D. J. Hinde, M. Dasgupta, C. R. Morton, L. R. Gasques, M. L. Brown, and M. D. Rodriguez, Phys. Rev. C **77**, 024606 (2008).

[38] R. G. Thomas, D. J. Hinde, D. Duniec, F. Zenke, M. Dasgupta, M. L. Brown, M. Evers, L. R. Gasques, M. D. Rodriguez, and A. Diaz-Torres, Phys. Rev. C **77**, 034610 (2008).
[39] D. J. Hinde, M. Dasgupta, J. R. Leigh, J. C. Mein, C. R. Morton, J. O. Newton, and H. Timmers, Phys. Rev. C **53**, 1290 (1996).
[40] J. F. Ziegler, M. D. Ziegler, and J. P. Biersack, Nucl. Instrum. Methods B **268**, 1818 (2010).
[41] A. Pal, S. Santra, P. C. Rout, Ramandeep Gandhi, Abhijit Baishya, T. Santhosh, R. Tripathi, and T. N. Nag, Phys. Rev. C **104**, L031602 (2021).
[42] D. J. Hinde, M. Dasgupta, J. R. Leigh, J. P. Lestone, J. C. Mein, C. R. Morton, J. O. Newton, and H. Timmers, Phys. Rev. Lett. **74**, 1295 (1995).
[43] D. C. Biswas, R. P. Vind, N. Kumar, Y. K. Gupta, R. V. Jangale, A. L. Inkar, L. A. Kinage, B. N. Joshi, S. Mukhopadhyay, G. K. Prajapati *et al.*, Nucl. Instrum. Methods A **901**, 76 (2018).
[44] R. du Rietz, E. Williams, D. J. Hinde, M. Dasgupta, M. Evers, C. J. Lin, D. H. Luong, C. Simenel, and A. Wakhle, Phys. Rev. C **88**, 054618 (2013).
[45] A. V. Karpov, A. S. Denikin, M. A. Naumenko, A. P. Alekseev, V. A. Rachkov, V. V. Samarin, V. V. Saiko, and V. I. Zagrebaev, Nucl. Instrum. Methods A **859**, 112 (2017).
[46] D. Hilscher and H. Rossner, Ann. Phys. Fr. **17**, 471 (1992).
[47] K. Hagino, N. Rowley, and A. T. Kruppa, Comput. Phys. Commun. **123**, 143 (1999).
[48] S. I. Mulgin, S. V. Zhdanov, N. A. Kondratiev, K. V. Kovalchuk, and A. Ya. Rusanov, Nucl. Phys. A **824**, 1 (2009).
[49] C. Böckstiegel, S. Steinhäuser, K.-H. Schmidt, H.-G. Clerc, A. Grewe, A. Heinz, M. de Jong, A. R. Junghans, J. Müller, and B. Voss, Nucl. Phys. A **802**, 12 (2008).
[50] R. Vandebosch and J. R. Huizenga, *Nuclear Fission* (Academic Press, New York, 1973), p. 324.
[51] A. Chatillon, J. Taïeb, H. Alvarez-Pol, L. Audouin, Y. Ayyad, G. Bélier, J. Benlliure, G. Boutoux, M. Caamaño, E. Casarejos *et al.*, Phys. Rev. Lett. **124**, 202502 (2020).
[52] K.-H. Schmidt, S. Steinhäuser, C. Böckstiegel, A. Grewe, A. Heinz, A. R. Junghans, J. Benlliure, H.-G. Clerc, M. de Jong, J. J. Muller *et al.*, Nucl. Phys. A **665**, 221 (2000).
[53] K.-H. Schmidt, B. Jurado, C. Amouroux, and C. Schmitt, Nucl. Data Sheets **131**, 107 (2016).